Dynamic Kosterlitz-Thouless transition in two-dimensional Bose mixtures of ultracold atoms

L. Mathey, Kenneth J. Günter, Jean Dalibard, and A. Polkovnikov

Phys. Rev. A **95**, 053630 — Published 24 May 2017

DOI: 10.1103/PhysRevA.95.053630

Dynamic Kosterlitz-Thouless transition in 2D Bose mixtures of ultra-cold atoms

L. Mathey[1,2], Kenneth J. Günter[3], Jean Dalibard,[3] and A. Polkovnikov[4]
[1] *Zentrum für Optische Quantentechnologien and Institut für Laserphysik, Universität Hamburg, 22761 Hamburg, Germany*
[2] *The Hamburg Centre for Ultrafast Imaging, Luruper Chaussee 149, Hamburg 22761, Germany*
[3] *Laboratoire Kastler Brossel, CNRS, UPMC, Ecole Normale Superieure, 24 rue Lhomond, F-75005 Paris, France*
[4] *Department of Physics, Boston University, 590 Commonwealth Ave., Boston, MA 02215*
(Dated: May 8, 2017)

We propose a realistic experiment to demonstrate a dynamic Kosterlitz-Thouless transition in ultra-cold atomic gases in two dimensions. With a numerical implementation of the Truncated Wigner Approximation we simulate the time evolution of several correlation functions, which can be measured via matter wave interference. We demonstrate that the relaxational dynamics is well-described by a real-time renormalization group approach, and argue that these experiments can guide the development of a theoretical framework for the understanding of critical dynamics.

I. INTRODUCTION

The understanding of non-equilibrium phenomena, in particular dynamic phase transitions, is an open frontier in many-body physics. While for equilibrium systems a rich variety of methods has been established, non-equilibrium systems are notoriously difficult to grasp, and a functioning conceptual framework is lacking. Given this state of research, ultra-cold atomic systems can play a crucial role in further understanding many-body dynamics. In fact, the unprecedented control of well-defined, isolated systems of ultra-cold atoms, has led them to be considered as 'quantum simulators' [1]: Cold atom systems are manipulated to create paradigmatic model systems of condensed matter physics, such as the Bose-Hubbard model [2], spin chains [3], the unitary Fermi gas [4], magnetic systems [5], the Dirac equation [6] and equilibration in one-dimensional (1D) gases [7]. The experimental measurements are cross-checked with theory, to guide the development of a theoretical framework [8].

In this paper, we propose to apply the concept of quantum simulation for a non-equilibrium setup, in particular for dynamic phase transitions. We present an implementation of the time-dependent renormalization group (RG) description, derived in [9], and demonstrate that it quantitatively predicts the dynamic evolution across a critical point, by comparing it to a numerical simulation. In particular, this proves the universality of the relaxational dynamics in this system, a concept well-established for equilibrium phase transitions, however not developed for dynamics in closed systems. Other RG treatments of non-equilibrium systems were reported in [10], other studies of quantum gas dynamics in 2D in Refs. [11].

We consider a system of weakly interacting bosons in two dimensions (2D), for a review see e.g. [12], which in equilibrium undergoes a Kosterlitz-Thouless (KT) phase transition as a function of temperature [13]. This system has two thermal phases, defined through the long-range behavior of the two-point correlation function $G(\mathbf{r}) \equiv \langle\psi^\dagger(0)\psi(\mathbf{r})\rangle$, where $\psi(\mathbf{r})$ is the particle annihilation operator at site $\mathbf{r}$. At low temperatures this function decays algebraically, $G(\mathbf{r}) \sim |\mathbf{r}|^{-\tau/4}$. The exponent τ increases monotonically from zero to 1 as the temperature is increased from zero to the critical temperature T_c. Above T_c, the functional form of $G(\mathbf{r})$ changes to exponential decay, $G(\mathbf{r}) \sim \exp(-|\mathbf{r}|/r_0)$, with a decay length r_0. This change is due to the deconfinement of vortex-antivortex pairs, and defines the KT transition. We trigger this transition dynamically by a quench, as described below. We find that after an intermediate time the system develops a metastable state in which the phononic modes have equilibrated, and $G(\mathbf{r})$ shows algebraic scaling with an exponent τ, which can be larger than the critical value 1. This exponent then increases slowly in time, until the correlation function changes to exponential scaling, indicating dynamic vortex deconfinement, cp. Ref. [16]. We demonstrate that the real-time evolution of $\tau(t)$ can be described by a real-time RG approach, by comparing it to our simulations. This constitutes a conceptually new insight into many-body dynamics. For the ultimate validation of this theoretical approach we propose a specific experimental setup in this paper.

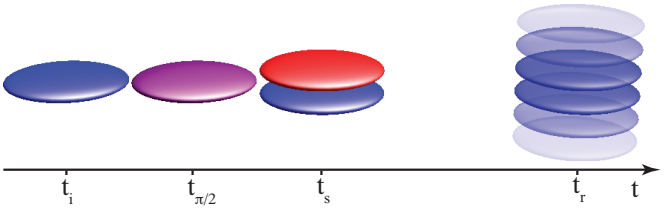

FIG. 1: Sketch of the interference protocol. We prepare a 2D atom cloud in state 1 at time t_i, and apply a $\pi/2$ pulse at $t_{\pi/2}$. We apply a field gradient at t_s, which separates state 1 (blue, lower cloud) and 2 (red, upper loud) spatially. We release the atoms at time t_r and measure their interference properties. Below, the time t will be given in units of J^{-1}.

The paper is organized as follows: In Sect. II we describe the interferometric measurement sequence. In Sect. III we discuss the numerical simulation, and in Sect. IV the numerical evidence for a dynamical Kosterlitz-Thouless transition. In Sect. V we demonstrate that our real-time renormalization group approach describes the long-time dynamics of the system, and in Sect. VI we conclude.

II. INTERFEROMETRIC PROTOCOL

In Fig. 1 we sketch the quench and measurement sequence. We consider a 2D gas of atoms, such as ^{87}Rb, at a temperature below T_c with an initial scaling exponent $\tau_i < 1$ in an internal state labelled 1. At a time $t_{\pi/2}$, a radio-frequency or microwave pulse drives the transition from state 1 to another state 2. The duration and intensity of the pulse are adjusted to provide a $\pi/2$ transition, so that the superfluid (SF) is now in the state $(\psi_1(\mathbf{r}) + \psi_2(\mathbf{r}))/\sqrt{2}$, where $\psi_1(\mathbf{r})$ and $\psi_2(\mathbf{r})$ are the single-particle operators of states 1 and 2. If the interaction strengths between 1 and 2 are identical (as they approximately are for the hyperfine levels of ^{87}Rb in its ground state), the rotation between the internal states is a symmetry of the system and the resulting SF state is still a steady state. Then at a later time t_s, we perform a quench of the gas by spatially separating the two species with a magnetic field gradient. This has the effect that the inter-species interaction is set to zero. For ^{87}Rb, the two hyperfine states could be $|F = 1, m_F = -1\rangle$ and $|F = 2, m_F = -1\rangle$, which have Landé factors of opposite sign. We note that if this quench is not sudden but has a non-zero ramp time, as below, the resulting light cone dynamics of Refs. [9, 16] will be washed out. However, the long time dynamics of the decay of the supercritical condensate depends primarily on the reduction of the density of each cloud by a 1/2, resulting in a lower critical temperature. These features of the dynamics are therefore robust under different choices of the ramp time. We measure the coherence properties at some release time t_r by (i) switching off the confinement along the initially frozen direction, so that the two gases expand along this direction and overlap; (ii) performing another $\pi/2$ pulse between 1 and 2; (iii) recording the atomic density in one of the two states, say 1, which reveals the matter-wave interference between the two planes. We note that 'splitting' of a 1D SF was discussed in [14].

III. NUMERICAL SIMULATION OF CONDENSATE DYNAMICS

We describe the system with the Hamiltonian $H = H_1 + H_2 + H_{12}$, where

$$H_a = \sum_{\mathbf{r}} l^D \Big[-\frac{\hbar^2}{2m}\psi_a^\dagger(\mathbf{r})\triangle\psi_a(\mathbf{r}) - \mu\psi_a^\dagger(\mathbf{r})\psi_a(\mathbf{r}) + \frac{g_0}{2}\psi_a^\dagger(\mathbf{r})\psi_a^\dagger(\mathbf{r})\psi_a(\mathbf{r})\psi_a(\mathbf{r})\Big], \quad (1)$$

and

$$H_{12} = \sum_{\mathbf{r}} l^D \Big[g_{12}\psi_1^\dagger(\mathbf{r})\psi_2^\dagger(\mathbf{r})\psi_2(\mathbf{r})\psi_1(\mathbf{r})\Big], \quad (2)$$

where the states are labeled $a = 1, 2$, and the dimension $D = 2$; l is the discretization length scale of this representation, see Ref. [15], i.e. the lattice constant of the Bose-Hubbard model. m is the atom mass, and g_0 (g_{12}) is the strength of the intra- (inter-) species contact interaction. For atoms confined to 2D motion by a harmonic potential in the third direction, these are approximately

$$g_0 = \frac{2\sqrt{2\pi}\hbar^2}{m}\frac{a_s}{l_0}; \quad g_{12} = \frac{2\sqrt{2\pi}\hbar^2}{m}\frac{a_{12}}{l_0}. \quad (3)$$

l_0 is the harmonic oscillator length $l_0 = (\hbar/m\omega_0)^{1/2}$ of the confining potential $m\omega_0^2 z^2/2$ in z direction; a_s and a_{12} are the s-wave scattering lengths. For hyperfine states of ^{87}Rb these are around 5 nm.

Initially all atoms are in state $a = 1$, and form a SF of total density ρ_0 at a temperature $T < T_c$. We describe this state with a Bogoliubov analysis based on the

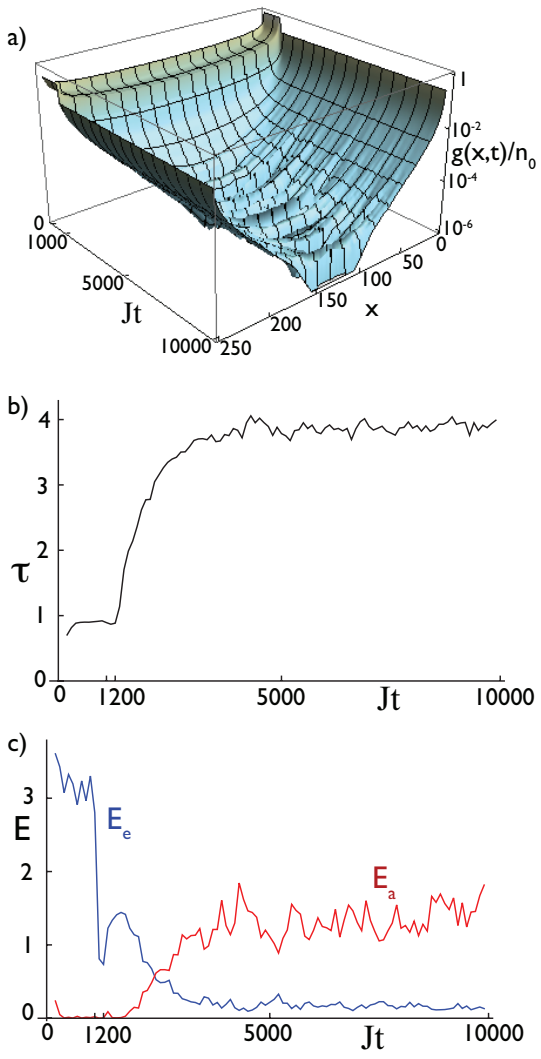

FIG. 2: a) $g_1(x,t)/n_0$ on a logarithmic scale, for $U/J = 0.25$ and $\tau_i = 0.89$ on a 250×250 lattice. The $\pi/2$ pulse is applied at $Jt_{\pi/2} = 1000$. U_{12} is turned off at $Jt_s = 1200$. After t_s, $g_1(x,t)$ gradually changes its functional form, from algebraic to exponential. b) Fitted algebraic exponent τ obtained from the data in a). c) Fitting errors E_e and E_a.

phase-density representation $\psi(\mathbf{r}) \approx e^{i\theta(\mathbf{r})}\sqrt{\rho_0 + \delta\rho(\mathbf{r})}$, see Ref. [15]. As mentioned, the correlation function $G_1(\mathbf{r}) \equiv \langle\psi_1^\dagger(0)\psi_1(\mathbf{r})\rangle$ decays algebraically, $G_1(\mathbf{r}) \sim |\mathbf{r}|^{-\tau/4}$, with

$$\tau^{-1} = \pi\hbar^2\rho_s/(2mT), \tag{4}$$

see Refs. [17, 18], implicitly defining the SF density ρ_s. Within the Bogoliubov approximation, $\rho_s = \rho_0$. However, based on Ref. [18], for weak interactions and away from the critical regime, an improved estimate is

$$\tau^{-1} \approx \pi\hbar^2\rho_0/(2mT) + C_0, \tag{5}$$

see [19], with $C_0 = (\ln(2gm/\hbar^2) - 1)/4$. We simulate the dynamics with a numerical implementation of the Truncated Wigner approximation (TWA), see e.g. Refs. [20, 21]. It is convenient to represent the system as a Bose-Hubbard model with two species $b_{a,i}$, where i is the lattice site, and $a = 1, 2$ the species index. The single-particle operators of the two representations are related as $b_{a,i} = l^{D/2}\psi_a(\mathbf{r}_i)$, where $\mathbf{r}_i$ is the real-space location corresponding to lattice site i. The tunneling energy J and m are related through $J = \hbar^2/(2ml^2)$; g_0, g_{12} and the Bose-Hubbard interactions through $U = g_0/l^D$ and $U_{12} = g_{12}/l^D$, respectively. We use $\hbar/J$ as the time unit and choose $U/J = U_{12}/J = 0.25$. Using the relation $U/J = \sqrt{32\pi}a_s/l_0$ from Eq. (3), this value corresponds to $l_0 \sim 200$nm, which is routinely achieved experimentally. We sample the initial state according to the Wigner distribution $W(x_\mathbf{k}, p_\mathbf{k}) \sim \exp(-x_\mathbf{k}^2/2\sigma_{x,\mathbf{k}}^2 - p_\mathbf{k}^2/2\sigma_{p,\mathbf{k}}^2)$, with $\sigma_{x,\mathbf{k}}^2 = 1/(2\omega_\mathbf{k}\tanh(\omega_\mathbf{k}/(2T_0)))$ and $\sigma_{p,\mathbf{k}}^2 = \omega_\mathbf{k}/(2\tanh(\omega_\mathbf{k}/(2T_0)))$, where T_0 is the initialization temperature, and the Bogoliubov modes $\beta_k = \sqrt{\omega_\mathbf{k}/2}x_\mathbf{k} + i/\sqrt{2\omega_\mathbf{k}}p_\mathbf{k}$. From these we construct $\delta\rho(\mathbf{r})$ and $\theta(\mathbf{r})$ and from these $\psi_1(\mathbf{r})$, see [22]. $\psi_2(\mathbf{r}_i)$ is initialized with vacuum fluctuations $\langle|\psi_2(\mathbf{r}_i)|^2\rangle = 1/2l^D$. The initial state is propagated by the equations of motion.

IV. DYNAMICAL KOSTERLITZ-THOULESS TRANSITION

In Fig. 2 a) we show $g_a(x,t) \equiv \langle b_{a,i}^\dagger(t)b_{a,i+x}(t)\rangle$ for $a = 1$ for a 250×250 lattice, for $n_0 \equiv l^D\rho_0 = 5$. We use $T_0/J = 7$ in the initialization, to let the system equilibrate to a SF with scaling exponent $\tau_i = 0.89$. We apply the $\pi/2$ pulse at time $Jt_{\pi/2} = 1000$; the density drops to half its initial value. At time $Jt_s = 1200$ we turn off U_{12}, see [24] and [25]. The evolution after the quench separates into two time domains. The system first relaxes to a metastable SF state, and then changes the functional form of the correlation function from algebraic to exponential on a much longer time scale, $t \approx 10^3\hbar/J$. To study this quantitatively, we fit the correlation function with two functions. We use $f_a(x) = C(\sin(\pi x/N)N/\pi)^{-\tau/4}$ with C and τ as fitting parameters to test for algebraic scaling. N is the number of lattice sites in one dimension. For large N, $f_a(x) \sim |x|^{-\tau/4}$. The fitted exponent τ is plotted in Fig. 2 b), and for a shorter time evolution and a 100×100 lattice as the blue dotted line in Fig. 3 a), see App. A. The constant value of τ before $t_{\pi/2}$ is τ_i of our physical initial ensemble. For exponential scaling, we use $f_e(x) = C\exp(-\kappa\sin(\pi x/N)N/\pi)$ with C and κ as fitting parameters. We define the fitting errors $E_{a,e} \equiv \sum_{i=1}^{N-1}(g(x,t) - f_{a,e})^2$. In Fig. 2 c), we show the fitting errors for the data plotted in Fig. 2 a). We recover

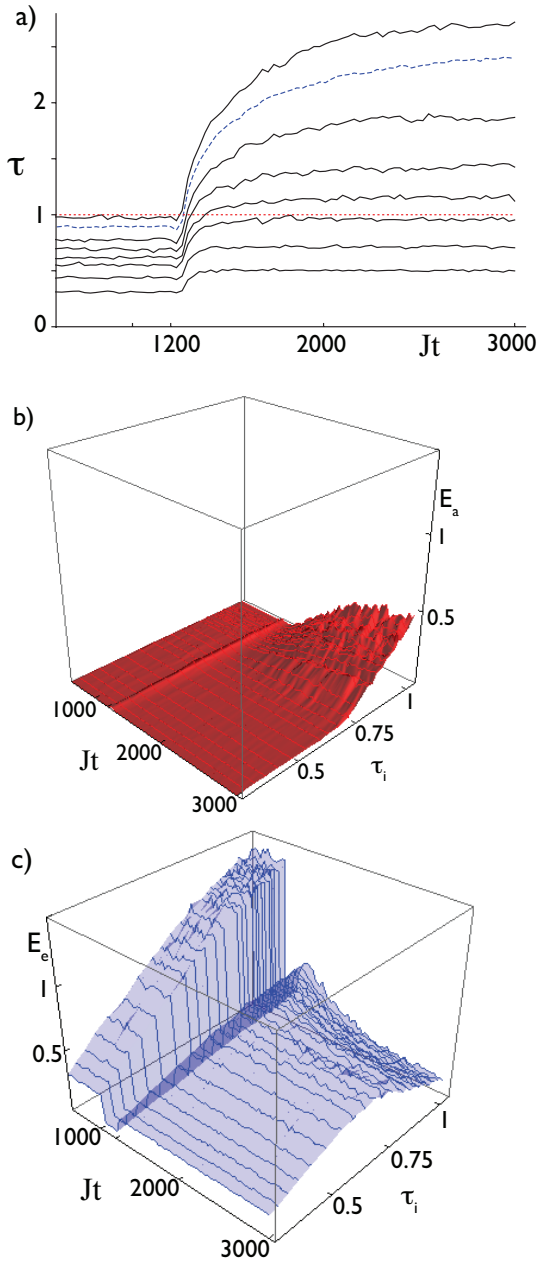

FIG. 3: a) Algebraic exponent $\tau(t)$ from fitting $g_1(\mathbf{x}, t)$ on a 100×100 lattice, for different τ_i. The red, dotted line is the critical value 1. The blue, dashed line is $\tau(t)$ for $\tau_i = 0.89$ (as in Fig. 2). b) Algebraic and c) exponential fitting errors $E_{a,e}$.

the time scales discussed above. (i) After the random draw of x_k and p_k and before the $\pi/2$ pulse, the system rapidly equilibrates in few tens of $\hbar/J$ and the two errors fluctuate around a ratio of $E_e/E_a \sim 100$, indicating that $g_1(\mathbf{x}, t)$ is much better fitted with an algebraic test function. (ii) After the $\pi/2$ pulse and before the quench, the density of species 1 drops to half its original value after $t_{\pi/2}$ but the gas is still in equilibrium. Both errors $E_{a,e}$ thus drop by a factor of 4, while maintaining the ratio ~ 100. (iii) After the quench, E_e decreases and E_a increases on a long time scale.

We repeat this calculation for different τ_i, and plot $\tau(t)$ and $E_{a,e}$ as a function of time and of τ_i, see Fig. 3. For small τ_i, $\tau(t)$ increases initially and then remains constant below 1, and $E_e/E_a \sim 10^2$. For $\tau_i \gtrsim 0.6$, $\tau(t)$ increases above 1, and does not remain constant, but shows a slow increase, Fig. 3 a). E_a grows, and becomes eventually larger than E_e, as shown in Fig. 3 b) and c), which indicates the functional form change of $g_1(\mathbf{x}, t)$. This demonstrates a dynamic KT transition. We also observe a time regime in which $\tau > 1$, but the change to exponential scaling has not yet occurred. This is the metastable, supercritical SF described in Refs. [9, 16]. Further we note that after the quench, the algebraic error briefly spikes up, see also Fig. 6. This is due to the light cone dynamics [9, 16, 23] triggered by the quench: After the quench, $g_1(x, t)$ is only piece-wise algebraic, i.e. it behaves as $|x|^{-\tau_1/4}$ for $|x| < c(t - t_s)$, and as $|x|^{-\tau_2/4}$ for $|x| > c(t - t_s)$, with differing exponents τ_1, τ_2; thus the fitting error is increased.

V. REAL-TIME RENORMALIZATION GROUP APPROACH

We now demonstrate that this transition can be captured with the RG approach derived in Ref. [9]. Its key statement is that the transition from the metastable, 'pre-thermalized' state to the fully-thermalized, vortex-deconfined state is described by the flow equations

$$\frac{dy}{d\ell} = 2(1 - 1/\tau)y; \quad \frac{d\tau}{d\ell} = 64\pi^2\alpha y^2/\tau \qquad (6)$$

where α is a non-universal constant, and y is the vortex fugacity, see [26] and [27]. ℓ is the flow parameter, related to real time by $t = t_0 e^{\ell}$, with some time constant t_0. We thus have to estimate the scaling exponent of the meta-stable state, referred to as τ^*, which we extract at the time $L/(2c)$, at which the light cone dynamics is completed. This exponent will drift slowly under the subsequent vortex unbinding dynamics, however this ambiguity is resolved by adjusting the initial value of the vortex fugacity, as described below. The system has two phononic sectors, corresponding to symmetric and anti-symmetric superpositions of phase and density excitations. Immediately after the quench, only the symmetric sector is thermally activated, whereas the anti-symmetric sector only displays vacuum fluctu-

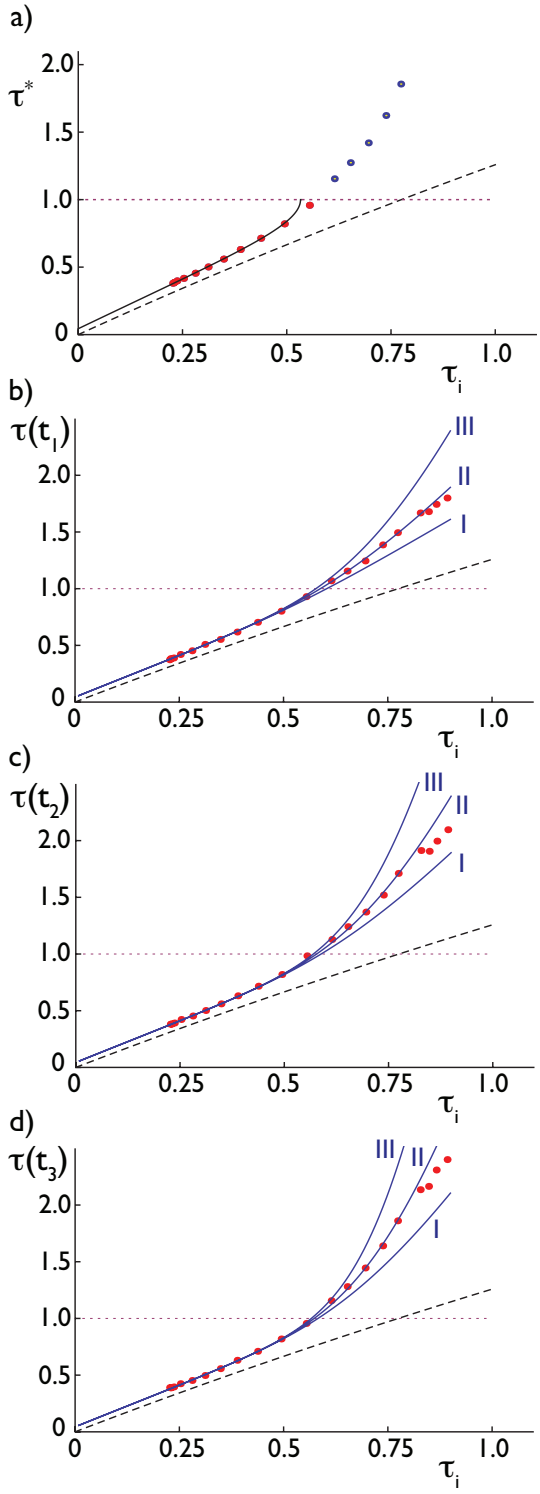

FIG. 4: a) Numerical data for τ, averaged over $Jt = [2100, 3000]$. The red, filled dots have $\tau < 1$, the dark circles have $\tau > 1$. The black, continuous line is τ_1^* with the optimal fitting parameters, fitted to the data $\tau < 1$. The red, dotted line indicates the critical line $\tau = 1$. The black, dashed line is $\tau_{\rm lin}^*$. b)-d) Numerical data τ at times $t_1 = 1500/J$, $t_2 = 2400/J$ and $t_3 = 2970/J$ (b-d) as a function of τ_i. The blue, continuous lines labelled I – III are in b) $\tau(\ell^* = 1.7)$, $\tau(\ell^* = 2.1)$ and $\tau(\ell^* = 2.5)$, respectively. In c) $\tau(\ell^* = 2.1)$, $\tau(\ell^* = 2.5)$ and $\tau(\ell^* = 2.9)$, respectively, and in d) $\tau(l^* = 2.3)$, $\tau(\ell^* = 2.7)$ and $\tau(\ell^* = 3.1)$, respectively. t_0 is $196.3/J$.

ations. We find that the two sectors thermally equilibrate on a short time scale of $\sim 10^2\hbar/J$, by calculating ratios of $g_s(\mathbf{x}) \equiv \langle\psi_1(0)^\dagger\psi_2(0)^\dagger\psi_2(\mathbf{x})\psi_1(\mathbf{x})\rangle$ and $g_a(\mathbf{x}) \equiv \langle\psi_1(0)^\dagger\psi_2(0)\psi_2^\dagger(\mathbf{x})\psi_1(\mathbf{x})\rangle$, such as $g_s(\mathbf{r})/g(\mathbf{r})^2$, $g_a(\mathbf{r})/g(\mathbf{r})^2$, $g_s(\mathbf{r})g_a(\mathbf{r})/g(\mathbf{r})^4$, etc, which all approach unity. This result differs from the behavior of 1D gases, for which the two sectors stay out-of-equilibrium for a much longer time [14]. To estimate τ^* analytically, we use energy conservation. For T much larger than the mean-field energy, the total energy scales as T^2. After the quench and equilibration, the resulting temperature is thus $T/\sqrt{2}$. We use Eq. (5) for τ, and note that the density is reduced by $1/2$, and find $\tau^*_{\rm lin} = (1/(\sqrt{2}\tau_i)+(1-1/\sqrt{2}) * C_0)^{-1}$, with $C_0 = (\ln(2gm/\hbar^2) - 1)/4$, for a 2D gas in continuum. However, C_0 will be renormalized for a discretized representation, see Ref. [18], and we use it as a fitting parameter. We show $\tau^*_{\rm lin}$ in Fig. 4 in comparison to the numerical data, with the optimal C_0 determined below. We use $\tau^*_{\rm lin}$ as the initial value for $\tau(0) = \tau^*_{\rm lin}$. To determine the initial value for the fugacity, we write the flow equation as $d(\alpha y^2)/dl = 4(1 - 1/\tau)(\alpha y^2)$. It is here that the slightly differing values of τ at different times can be compensated for by choosing different values of the fugacity, which resolves the ambiguity. The quantity $(\tau - 1)^2 - 32\pi^2\alpha y^2$ is invariant under the flow, and thus the asymptotic value for τ^* below the critical point is $\tau^*(\infty) = 1 - ((\tau - 1)^2 - 32\pi^2\alpha y^2)^{1/2}$. This motivates to use $\tau^*_1 = 1 - ((\tau^*_{\rm lin} - 1)^2 - 32\pi^2 A)^{1/2}$ as a fitting function for C_0 and $A = \alpha y^2(0)$. In addition, we use t_0 as a global fitting parameter for the three data sets of Fig. 4. In Fig. 4 a) we show τ^*_1, with $C_0 = 0.299$ and $A = 2.7\times10^{-4}$, and the numerical data for τ averaged over the time range $Jt = [2100, 3000]$. We use these values in our initial conditions. We integrate the flow equations to different values ℓ^*, in particular to $0, 0.1, 0.2, ..., 4.0$. In Figs. 4 (b-d) we show the numerical results for τ at the times $t_1 = 1500/J$, $t_2 = 2400/J$ and $t_3 = 2970/J$, each averaged over a time interval of $60/J$. We determine the value of t_0 for which the functions $\tau(\ell^*)$ fit the numerical results the closest. The ratios t_i/t_j are approximately $\exp(\ell_i/\ell_j)$, but we note that because of the logarithmic dependence of ℓ on t, a large numerical uncertainty is present. We show the optimal $\tau(\ell^*)$, and two close-by solutions for visual comparison. We find that the RG flow well describes the critical dynamics.

VI. CONCLUSIONS

In conclusion, we have presented a realistic experiment to investigate the dynamic KT transition in ultra-cold gases in 2D. We demonstrate that the critical dynamics can be described by the RG approach developed in Ref. [9], as it predicts correctly the dynamic evolution found in the TWA simulation. The time evolution of the correlation functions can be detected via interference measurements discussed in Ref. [12]. As we show in App. C, these results also hold for a quantum gas in a box potential. These predictions and their experimental verification would pave the way to an RG-based theory framework for critical dynamics.

VII. ACKNOWLEDGMENTS

LM acknowledges support from the Deutsche Forschungsgemeinschaft through the SFB 925 and the Hamburg Centre for Ultrafast Imaging, and from the Landesexzellenzinitiative Hamburg, which is supported by the Joachim Herz Stiftung. AP was supported by NSF DMR-0907039, AFOSR FA9550-10-1-0110, and the Sloan Foundation. K-J G and JD were supported by IFRAF and ANR (BOFL project).

[1] R. Feynman, Int. J. of Th. Physics, **21**, 467 (1982).
[2] W. S. Bakr, *et al.*, Science **329**, 547 (2010).
[3] J. Simon, *et al.*, Nature **472**, 307 (2011).
[4] K. Van Houcke, *et al.*, Nature Phys. **8**, 366 (2012).
[5] J. Struck, *et al.*, Science **333**, 996 (2011).
[6] R. Gerritsma, *et al.*, Nature **463**, 68 (2010).
[7] S. Trotzky, *et al.*, Nature Physics **8**, 325 (2012).
[8] H. Weimer, *et al.*, Nature Phys. 6, 382-388 (2010); M. Ortner, *et al.*, New J. Phys. 11, 055045 (2009); M. Lewenstein, *et al.*, Adv. in Physics **56**, 243, (2007); H. P. Büchler, *et al.*, Phys. Rev. Lett. **95**, 040402 (2005); N. Szpak, R. Schützhold, New J. Phys. **14**, 035001 (2012); L. Mazza, *et al.*, New J. Phys. **14**, 015007 (2012); H. Weimer, *et al.*, Quantum Information Processing **10**, 885 (2011); Z. Lan, *et al.*, Phys. Rev. B **84**, 165115 (2011).
[9] L. Mathey and A. Polkovnikov, Phys. Rev. A 81, 033605 (2010).
[10] A. Mitra and T. Giamarchi, Phys. Rev. B **85**, 075117 (2012); Phys. Rev. Lett. **107**, 150602 (2011); E. G. Dalla Torre, *et al.*, Nat. Phys. **6**, 806 (2010).
[11] J. Hofmann, *et al.*, Phys. Rev. Lett. **113**, 095702 (2014); K. Damle, *et al.*, Phys. Rev. A **54**, 5037 (1996).
[12] Z. Hadzibabic and J. Dalibard, Rivista del Nuovo Cimento **34**, 389 (2011).
[13] J. M. Kosterlitz and D. J. Thouless, J. Phys. C **6**, 1181 (1973); V. S. Berezinskii, Sov. Phys. JETP **34**, 610 (1972).
[14] T. Kitagawa, *et al.*, New J. Phys. **13** 073018 (2011); M. Gring, *et al.*, Science **337**,1318 (2012).
[15] C. Mora and Y. Castin, Phys. Rev. A **67**, 053615 (2003).
[16] L. Mathey and A. Polkovnikov, Phys. Rev. A 80, 041601(R) (2009).
[17] N. Prokof'ev, *et al.*, Phys. Rev. Lett. 87, 270402 (2001).
[18] N. Prokof'ev and B. Svistunov, Phys. Rev. A 66, 043608 (2002).
[19] We ignore the conceptually important, but numerically small difference between ρ_s in Eq. 4 and the SF density discussed in Ref. [18], as pointed out in N. Prokof'ev and B. Svistunov, Phys. Rev. B 61, 11282 (2000).
[20] P. B. Blakie, *et al.*, Adv. in Phys. **57**, 363 (2008).
[21] A. Polkovnikov, Annals of Phys. 325, 1790 (2010).
[22] To avoid the rare event of a negative density fluctuation, we truncate the distribution of $\delta\rho(\mathbf{r})$ to $-\rho_0$ from below. To ensure that the density expectation value is ρ_0 we truncate $\delta\rho(\mathbf{r})$ to $+\rho_0$ from above.
[23] P. Calabrese and J. Cardy, Phys. Rev. Lett. **96**, 136801 (2006); J. Stat. Mech. - Theor. and Exp., P06008 (2007).
[24] We use $U_{12}(t) = U(1-\tanh((t-t_s)/\Delta t_s))/2$ with $J\Delta t_s = 5$. For the example $\Delta t_s = 1.4$ ms.
[25] To describe a 2D cloud with $\rho_0 = 50/(\mu\text{m})^2$, we have to choose $l = 0.32\,\mu$m. For ^{87}Rb, $\hbar/J$ is then 0.28ms. The phonon velocity of each cloud after the quench is $c = 1.3$mm/s.
[26] Over the temperature range considered here, we ignore the temperature dependence of y. We also ignore the renormalization of the phonon velocity, see Ref. [9], expected to be only a small correction.
[27] In this coarse-grained formulation, no explicit dissipative term appears, in contrast to Ref. [10]. However, a redistribution of energy is included through the conservation of adiabatic invariants, see [9].
[28] Laura Corman, Lauriane Chomaz, Tom Bienaime, Remi Desbuquois, Christof Weitenberg, Sylvain Nascimbene, Jean Dalibard, Jerome Beugnon, Phys. Rev. Lett. **113**, 135302 (2014); A. L. Gaunt, T. F. Schmidutz, I. Gotlibovych, R. P. Smith, and Z. Hadzibabic, Phys. Rev. Lett. **110**, 200406 (2013).
[29] Amy C. Mathey, Charles W. Clark, L. Mathey, Phys. Rev. A **90** 023604.

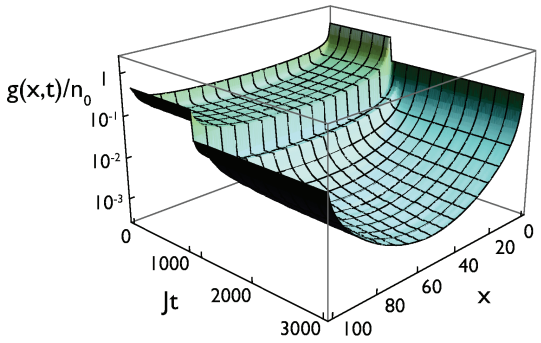

FIG. 5: Single-particle correlation function $g(x,t)$ for $\tau_i = 0.89$, for a 100×100 lattice.

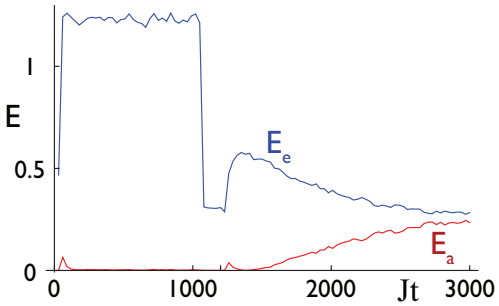

FIG. 6: Algebraic and exponential fitting errors $E_{a,e}$ for $\tau_i = 0.89$, for a 100×100 lattice.

Appendix A: Example for a 100×100 lattice

We show the single-particle correlation function $g(x,t)$ for a 100×100 lattice, for $\tau_i = 0.89$ in Fig. 5, for a time interval of $Jt = [0, 3000]$. The $\pi/2$ pulse is applied at $Jt_{\pi/2} = 1000$, where the density drops to half, and the quench is applied at $Jt_s = 1200$. As described in the main text, we fit this correlation function with an algebraic and an exponential fitting function. The algebraic fit gives $\tau(t)$ which is depicted as a blue, dashed line in Fig. 3 a) of the main text. In Fig. 6 we show the two fitting errors for the data shown in Fig. 5. We see the same behavior as for the example in Fig. 2 in the main

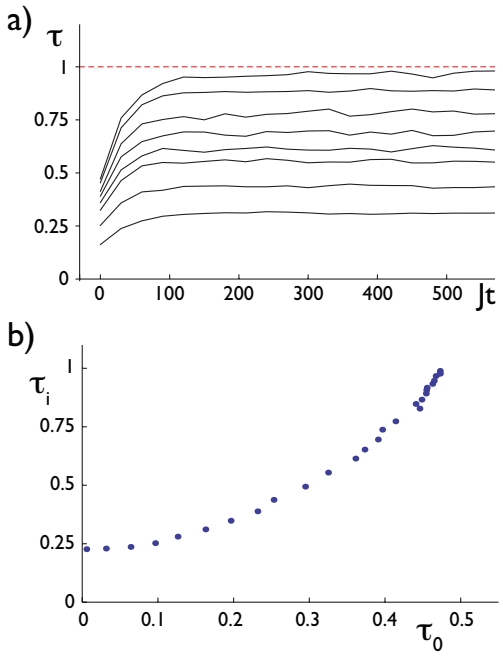

FIG. 7: In panel (a) we show the relaxation of the state before the time evolution to the state that is uses as the initial state of the simulation. In panel (b) we depict the power-law exponent of the state at the end of this relaxation as a function of the power law exponent before the relaxation.

text, but due to the shorter integration time the intermediate time behavior is better resolved, and because of the smaller system size the numerical uncertainty is reduced. Before the $\pi/2$ pulse, the ratio $E_e/E_a \sim 10^2$, after the pulse each error drops to a quarter of its value while maintaining the same ratio. After the quench at $Jt_s = 1200$, the ratio is initially of that same magnitude, but then changes on a much longer time scale. On an intermediate time scale, there is a metastable regime in which the correlation function is better fitted algebraically, but the exponent τ is much larger than 1, i.e. the system is supercritical. To construct the data shown in Fig. 3 of the main text, we repeat calculations as shown in Fig. 5, for a 100×100 lattice, and for different τ_i, and we determine $\tau(t)$, $E_a(t)$ and $E_e(t)$ from them.

Appendix B: Initialization

As described in the main text, we initialize the simulation with an ensemble of Bogoliubov modes, with an initial temperature T_0. We extract the power-law exponent τ_0 of this initial state. We then evolve the system under the equations of motion, until an equilibrated state is reached. This is state that we use as the initial state of the physical system. We extract the power-law exponent during the relaxation, as shown in Fig. 7 a), and we show the exponent of the equilibrated system, τ_i, in Fig. 7.

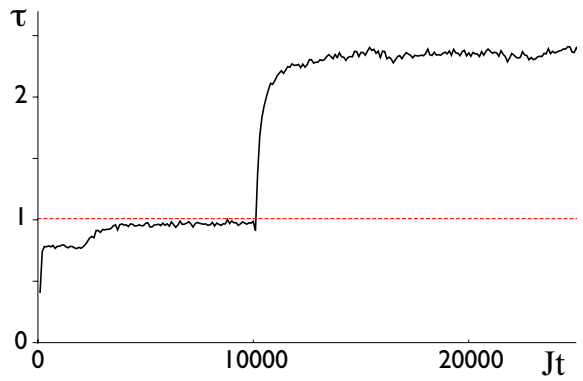

FIG. 8: We show the time evolution of the power law exponent τ as a function of time. The system is initialized as a homogeneous system at $Jt = 0$. Then, around $Jt_{t0} = 3000$, the box potential is ramped up. The system equilibrates to a steady state, with an exponent around $\tau \approx 0.95$. The quench is performed at $Jt_s = 10000$. The value of τ becomes supercritical, and the system develops exponential scaling around $Jt \approx 13000$.

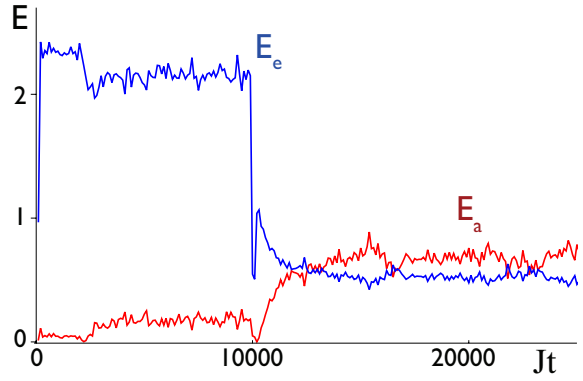

FIG. 9: Time evolution of the fitting errors E_e and E_a as a function of time.

Appendix C: Trapped system

In this section we demonstrate that the dynamical evolution that was described in the main text equally emerges in an atomic cloud in a trap. We consider a box potential, similar to the ones that were reported in Refs. [28]. The trapping potential is given by

$$\begin{aligned} V_{tr}(i_x, i_y) \;=\; V_0\Big(& (\tanh((x-L)/x_{tr})+1)/2 \\ & +(\tanh(-x/x_{tr})+1)/2 \\ & +(\tanh((y-L)/x_{tr})+1)/2 \\ & +(\tanh(-y/x_{tr})+1)/2\Big) \end{aligned} \tag{C1}$$

The spatial variables x and y are related to the lattice sites via $x = li_x$ and $y = li_y$. The site indices i_x and i_y run from 0 to $N-1$, where N is the lattice size, for which we choose $N = 150$. L is the system size, given by

$L = l(N-1)$. In the example shown in this section, we choose $V_0/J = 100$ and $x_{tr} = l$. The latter corresponds to $x_{tr} = 1\mu$m, and describes the length scale on which box potential rises. To create the initial state of the trapped system, we proceed similar to Ref. [29]. We first generate the equilibrium state of the homogeneous system with periodic boundary conditions, as described in the main text. Then we turn the trapping potential, Eq. C1, on, in a nearly adiabatic fashion, by using the ramp up function

$$f(t) \;=\; (\tanh((t-t_{to})/\Delta t_{to}) + 1)/2 \qquad \text{(C2)}$$

The time t_{to} is the turn-on time of the trap, and Δt_{to} is the time scale of the turn-on process. We choose $Jt_{to} = 3000$ and $J\Delta t_{to} = 500$. So the additional term in the Hamiltonian that describes the trapping potential, including its ramp up function, is

$$H_{tr} \;=\; f(t) \sum_{\mathbf{r},a} l^D V(i_x, i_y) \psi_a^\dagger(\mathbf{r}) \psi_a(\mathbf{r}) \qquad \text{(C3)}$$

with $\mathbf{r} = (x, y)$.

The resulting state, after it has equilibrated, is the initial state of the physical question that we address. We perform the $\pi/2$ pulse at $Jt_{\pi/2} = 9800$ and the quench at $Jt_s = 10000$. As for the previous examples, we compute the correlation function $G_1(\mathbf{r})$. Here, we calculate it in the bulk of the system, and exclude the regime near the edge of the box potential, with a distance of $5l$ away from the edge. As before, we extract the power-law exponent τ as a function of time, and the fitting errors. These are shown in Fig. 8 and 9. We find a qualitatively similar behavior to the case of a homogeneous system. This demonstrates that the dynamical evolution that we discuss in this paper is robust in the presence of a trap.